STABILITY OF THE AIR FLOW IN A TWO AISLE CABIN MODEL

M. Kühn, J. Bosbach, C. Wagner
German Aerospace Centre/Institute of Aerodynamics and Flow Technology
Bunsenstrasse 10, 37073 Göttingen
Germany

OVERVIEW

Mixed convection has been investigated experimentally in a mock-up representing a two-aisle cabin of a passenger aircraft mock-up at full scale. The layout and dimensions of the mock-up's interior have been deduced from the upper deck of the Airbus A380. Large scale Particle Image Velocimetry (PIV) and temperature field measurements were performed in one cross section of the cabin mock-up. With PIV the flow fields for two different air inlet configurations were measured and analysed under isothermal and cooling conditions. Furthermore the flow rates at the different air inlet positions were varied realizing a constant air exchange rate.

Results of the experimental parameter study are presented demonstrating that the stability of air circulation in an aircraft cabin is affected by different physical effects. It is found that the interaction between the air jets, the influence of buoyancy forces acting on the air jets and the interaction of the air jets with thermal plumes control the air flow and temperature distribution within the cabin.

1. INTRODUCTION

During the last decades the thermal loads in modern passenger airplanes have tremendously increased; so has the passenger's expectance with respect to a comfortable environment. Thus, the air conditioning system has to remove the produced heat to provide a comfortable temperature level inside the cabin. The thermal comfort of passengers is mainly influenced by the velocity and temperature distribution. In aircraft cabins the forced convection entering the cabin through the air inlet and thermal convection induced by the heat sources like e.g. the passengers are counteracting. Therefore the stability of circulating flow structures in this type of mixed convection depends on the interaction of buoyancy forces with the momentum of the incoming jet flows. To improve the understanding of the underlying physical mechanisms and their impact on the resulting velocity and temperature distributions, detailed numerical and experimental investigations of this kind of airflows are urgently needed.

Most of the experimental investigations conducted in this field so far had the aim to develop measurement techniques which provide the information needed for the improvement of the thermal comfort inside an aircraft cabin. In this respect mainly optical non-instructive measurement methods have emerged providing the two-dimensional flow fields in selected cross sections or three-dimensional volume segments of the cabin.

Müller et al. (1997) applied the Particle Tracking Velocimetry (PTV) technique using helium filled soap bubbles (HFSB) as tracer particles to investigate the air flow in an A330/A340 cabin. They obtained velocity vectors in one half of the cabin with a light sheet of 0.7 m thickness and compared their results favourably to computed flow fields which were generated using a Computational Fluid Dynamics (CFD) method. Later Müller et al. (2000) investigated the flow field in a preliminary A3XX upper deck cabin section by means of Particle Image Velocimtry (PIV) using an improved helium bubble generator. The light sheet was generated with halogen lamps introducing an additional heat span in one half of the cabin section. The obtained flow field was analysed and qualitatively compared with CFD results.

Mo et al. (2003) carried out PIV of the flow in a section of a B737 aircraft cabin. In their measurements they used microspheres of thermoplastic shells filled with a gas. Velocity and turbulence profiles were measured in nine planes in the vicinity of one thermal dummy build with a certain number of 0.61 x 0.61 m² patches. In their paper they present and discuss selected result which were obtained in one of the investigated planes.

A Particle Streak Velocimetry (PSV) technique for three-dimensional flow field measurements was developed by Sun et al. (2005). They investigated the flow in a wooden B767 mock-up section. The PSV results are the outcome of a parameter study comprising temperature variations of supplied air and the walls, occupation scenarios of the cabin with thermal dummies and obstructions which are discussed in Zhang et al. (2005). The focus of their work was on the air speeds induced in the vicinity of the passenger due to breathing.

Additionally, several groups conducted numerical simulations of cabin air flows investigating selected problems associated with aircraft's ventilation system. To do so CFD programs were developed and validated to show that they are able to reliably predict mixed convection in cabin. DeJager et al. (1992) for example used CFD to design an air inlet nozzle used in an aircraft cabin and studied the flow for different conditions. The numerical predictions were validated comparing the results with 106 local velocity measurements obtained from hot wire anemometry.

A three-dimensional simulation method to compute mixed convection in aircraft cabins was developed by Mizuno et al. (1992). They verified their results which were obtained in various simulations comparing them to local velocity measurements performed at points 12 inch apart in two cross sections within a B737 cabin mock-up and to temperature and CO_2 concentration measurements.

Singh et al. (2002) applied a CFD method to compute the flow within of a section of an aircraft cabin to study effects resulting from occupant heat loads. They investigated and discussed velocity, turbulence kinetic energy and temperature profiles and showed that the spreading of the supplied cabin air jets increases due to the emitted heat loads of occupants.

More recently Lin et al. (2005a) and Lin et al. (2005b) performed Reynolds-Averaged Navier-Stokes (RANS) simulation and Large Eddy Simulations (LES) of the flow to predict the dispersion of airborne pathogens in aircraft cabin. In Lin et al. (2006) they also compared instantaneous velocity components and energy spectra obtained in their LES of the flow in a generic cabin model with stereoscopic PIV results at five different locations showing that the results agree well with measurements.

Finally, Bosbach et al. (2006) and Günther et al. (2006) studied the flow field in a generic aircraft cabin and a sleeping bunk comparing PIV and CFD results with aim to identify reliable turbulence models for numerical prediction of mixed convection in aircraft cabins.

In the present paper we present the PIV results and temperature fields obtained in a parameter study varying the flow rates and the location of operated cabin inlets in a generic but realistic model of a two aisle airplane cabin mock-up at full scale to study the stability of the air circulation.

2. PASSENGER AIRCRAFT CABIN MODEL

The aircraft cabin mock-up was designed as a generic replica of a section of the Airbus A380 upper deck. Compared to the latter the dimensions are slightly reduced with a width of 5.1 m, length of 6 m and a maximum height of 2.2 m. Five seat rows are installed in the mock-up, with two seats on both sides and four in the middle, separated by two aisles as presented in Fig. 1. On each of the 40 seats one thermal passenger dummy is seated. Additionally, the mock-up is equipped with generic overhead bins on the lateral and the middle ceiling positions. Further, in total 36 air inlets are installed in six lines consisting of six inlets with a dimension of 18 mm x 920 mm each. The positions of the lines of air inlets are shown in Fig. 1. 24 air inlets or two lines of air inlets can be operated together. The air leaves the cabin through twelve air outlets, each having a size of 50 mm x 900 mm. They are located 50 mm above the cabin floor. The amount of incoming and outgoing air is controlled by a control system with 18 flaps and measuring orifices.

The 40 passenger dummies are equipped with internal heaters each of which are equipped with one 15 W bulb in the throat and one 40 W bulb in the breast. The resulting 55 W each dummy emits correspond to the thermal load of a passenger in a real cabin if perspiration is neglected. Moreover four electrical heating panels on the top and the sides, see Fig. 1, with a width of 100 mm each and a total power of 1.8 kW, are installed to simulate the heat emission of the light bands. The electrical heating devices are all working in constant heat flux mode. Finally, glass windows at the front and the back of the mock-up allow the optical access in the mock-up which is needed for PIV and flow visualisation.

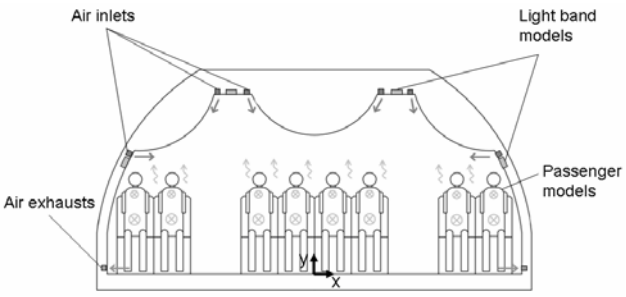

FIG 1. Cross section of the generic aircraft passenger cabin mock-up

The measurements described below have been conducted for the following two inlet configurations. For configuration A the inner ceiling air inlets and the lateral air inlets were operated whereas configuration B denotes that the two ceiling air inlets were operated together. All air inlets were oriented parallel to the respective overhead bin contour. The air exchange rate of the mock-up was set to a constant value of 23 litre/h which corresponds to a flow rate of 27 m³/h per passenger and 300 litre/s in total, respectively.

In order to investigate the air flow pattern for different inflow boundary conditions the relative volume/mass flow between the different air inlets were varied systematically according to Tab. 1. Additionally in Tab. 1 the names for the different configurations that are used in the following are defined. The respective denoted total volume flow for one air inlet position is equally distributed to the left and right hand cabin side.

Configuration	Inner ceiling inlets, liter/s	lateral air inlets, liter/s	outer ceiling air inlets, liter/s
A 50/50	150	150	0
A 33/67	100	200	0
A 67/33	200	100	0
B 50/50	150	0	150
B 33/67	100	0	200
B 67/33	200	0	100

TAB 1. Definition of test configurations and operating different air inlets and different volume flow rates

All six scenarios have been investigated under isothermal conditions, for which all heat sources were switched off, and under cooling conditions with the passenger dummies and the light band models switched on, i.e. with a heating power of 4 kW in total. By switching from the isothermal to the cooling case we were able to study the influence of buoyancy effects on the flow. Under cooling conditions, where the incoming air jets enter a warm cabin, the temperature difference between the cabin air and the incoming air amounted to $\Delta T = 6.4 \pm 0.4$ K.

FIG 2. Snapshot of the surface temperature differences with respect to the mean cabin temperature of passenger dummies and the cabin measured by infrared thermography for configuration A 50/50.

Infrared thermography measurements of the resulting surface temperatures of the passenger dummies and the light band models have been performed. The resulting surface temperature distribution obtained for configuration A 50/50 is presented in Fig 2. It turned out that the surface temperatures are almost identical for any of the investigated configurations. Due to the applied constant heat flux mode the temperatures are biased by the average cabin air temperature. Therefore, only the temperature differences ΔT_C with respect to the mean cabin air temperature are plotted in Fig. 2. The passenger dummies reveal average surface temperatures of approximately ΔT_C = 10 K in the head region, which decrease on the clothes and the arms to approximately ΔT_C = 5 K. Since the legs of the passenger models are not heated, they take on the cabin air temperature. The lateral light band models reveal surface temperature differences of ΔT_C = 45 K, while the light band models at the ceiling exhibit temperature differences of ΔT_C = 55 K.

A permanently installed temperature measurement system consisting of 36 k-type thermocouples was used to record the temperature boundary conditions during all measurements. The temperature of the incoming, outgoing and ambient air was measured at 22, 8 and 1 position, respectively. Moreover at five locations in the mock-up the temperature was measured to evaluate the average mock-up temperature.

3. EXPERIMENTAL SET-UP

3.1. Large scale PIV set-up

To measure the velocity distribution in a cross section of the cabin mock-up Particle Image Velocimetry (PIV) (see e.g. Raffel et al. (1997)) was applied. In Fig. 3 the PIV set-up is illustrated. To illuminate tracer particles in a plane of the mock-up a pulsed water-cooled Nd:YAG double oscillating laser (Brilliant Twins, Quantel) with a pulse energy of 350 mJ/pulse was used. Its beam was enlarged by a telescope, a combination of a concave (f = -150 mm) and convex lens (f = 500 mm), and afterwards extended by a cylindrical lens (f = -25 mm) to a light sheet with an opening angle of approximately 40° and a thickness of 3 - 5 cm in the observation area. Through a slit in the floor of the mock-up covered with glass the light sheet was coupled into the cabin whereas it spanned a plane of about 3.1 x 2.3 m² which is larger than half the cabin cross section.

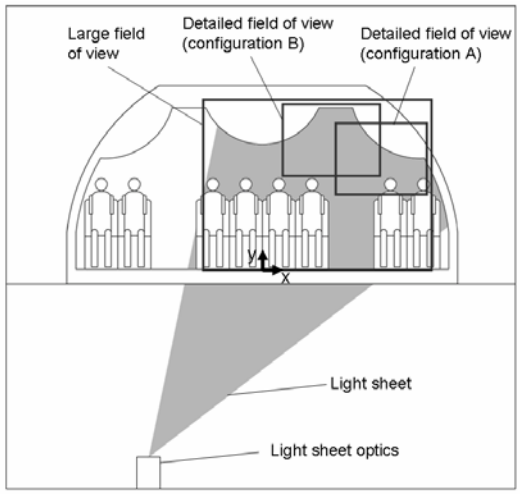

FIG 3. Optical set-up for PIV measurements in the cabin mock-up over two floors

Since the scattering of oil droplets which are normally used for PIV measurement is a too weak due to their tiny diameter of 1µm, we used helium filled soap bubbles (HFSB) as tracer particles which are suitable for large scale measurements. A home-made HFSB generator with three orifice type nozzles was used to produce bubbles with a diameter of 0.2 - 0.3 mm. For a detailed description of the HFSB generator and the characteristics of the HFSB the reader is referred to Bosbach et al. (2007). The settings of the generator can be adjusted in a way that the produced HFSBs are neutrally buoyant which results in an ideal following behaviour of the surrounding air flow (Müller et al. (2001)). Even if the HFSB are produced with a low momentum nozzle (Bosbach et al. (2007)) they are directly injected in the incoming air jet near the air inlets to avoid disturbing the flow field and to obtain proper mixing with the air in the cabin by turbulence. Thus, a homogenous tracer particle distribution in the cabin air flow could be realized.

The scattered light of the tracer particles resulting from two delayed laser pulses were recorded by two CCD cameras (Sensicam QE, PCO) with a Peltier cooled CCD sensor at a resolution of 1376 x 1024 each in parallel. One camera operating with a 21 mm lens (Distagon T* 2.8/21, Carl Zeiss) was used to scan the whole light sheet. A second camera with a 50 mm lens (Planar T* 1.5/50, Carl Zeiss) was employed to resolve details air jets near the air inlet, see Fig. 3.

To account for low frequency phenomena that occur in mixed convection flows (Bosbach et al. (2006) ?) nearly all measurements were performed with a frequency of 0.2 Hz whereas 360 double frame pictures were recorded by each camera. A smaller part of the measurements reconstruction was used to determine the displacement with sub-pixel accuracy. The interrogations were performed with a frequency of 2.5 Hz over a period of 64 s to observe the large field of view only. In the following all measurements were performed with this frequency if not stated otherwise.

In order to evaluate the velocity fields the local cross correlation using a multi pass interrogation algorithm has been applied to the interrogation windows of subsequent images. For noise reduction a minimum image of a sequence was subtracted previously and double correlation was performed. The interrogation window sizes were 31 x 31 mm² and 74 x 74 mm² in real space for the small and large field of view, respectively. The overlap of the interrogation windows were set to 50 percent.

3.2. Temperature field measurement set-up

Since the temperature distribution is important for the thermal comfort of aircraft passengers we have measured the temperature field in the aircraft cabin mock-up as well. For this purpose a horizontal temperature sensor rank consisting of 26 k-type thermocouples was used. The temperature distribution was determined by scanning 60 percent of the plane in which the velocity measurements were carried out with a spatial resolution of 70 x 70 mm².

In each horizontal position the temperature was recorded with 1/15 Hz and averaged over a time period of ten minutes resulting in a total measurement time of approximately five hours. Due to the fact that the ambient mock-up temperature could not be held constant the mock-up reaches only a quasi-stationary state. By reaching this state the difference between the average mock-up temperature and the temperature of the incoming air increases slightly by 0.12 K/h. The effect of this temperature drift on the measured velocity field can be neglected, since the PIV were performed for approximately 30 min.

4. RESULTS OF THE PARAMETER STUDY

In this section the results of the parametric study are discussed. The analyses concentrates on configuration A and afterwards on configuration B (see Tab. 1). Line plots are generated to allow for a quantitative comparison of the results obtained for the different configurations.

4.1. Results for Configuration A

4.1.1. Isothermal case

To analyse the topology of the flow field obtained for configuration A under isothermal conditions the averaged velocity field for the isothermal case A 50/50 are depicted in Fig. 4. The corresponding root mean square of the fluctuating velocity field (RMS) is presented in Fig. 5.

After entering the cabin the incoming air jets attaches directly to the overhead bins due to the Coanda effect. The jet supplied by the lateral air inlet follows the contour until reaching the ceiling where it gets entrained by the ceiling air jet. Following the central over head bin the merged jets form a stagnation point as they meet their counterpart from the left hand side of this cabin cross section, are combined and deflected to the floor. A second stagnation point, not visible in the PIV result, develops as the flow divides into two parts, both of which are following the cabin floor until they reach the air outlets.

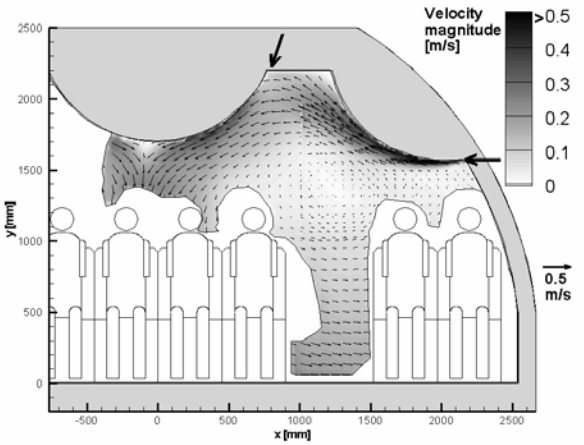

FIG 4. Mean velocity distribution of the air flow in the aircraft passenger cabin mock-up for configuration A 50/50 studied with large-scale 2C-2D PIV under isothermal conditions.

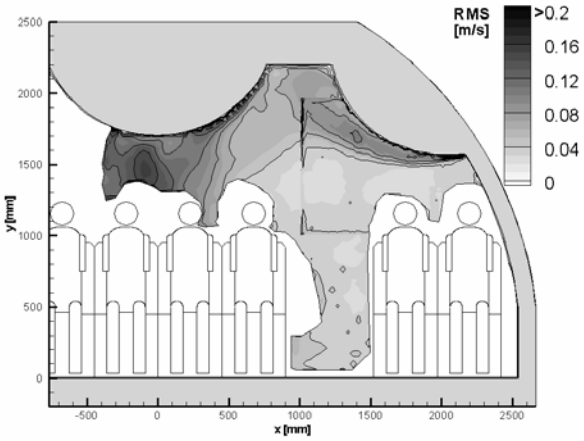

FIG 5. RMS velocity fluctuations of the air flow in the aircraft passenger cabin mock-up for configuration A 50/50 studied with large-scale 2C-2D PIV under isothermal conditions.

The RMS velocity field (Fig. 5) reflects higher RMS values (RMS > 0.08 m/s) in the pathways of the jets and lower values (RMS < 0.035 m/s) in the region away from the jets. Locally increased RMS values (RMS up to 0.15 m/s) in the vicinity of the visible stagnation point reveal that at this point the flow is highly time-dependent.

By varying the relative flow rate at the inlets which corresponds to a decrease of the momentum it is has been observed that the air jet separates before it reaches the ceiling. For the higher lateral flow rate (configuration A 33/67) the air jet velocity is larger close to the ceiling (not shown). The premature separation is a result of the entrainment of ambient fluid to the jet originating at the ceiling air inlet. The lateral air jet follows the wall and looses momentum due to the wall shear stresses. This leads after a critical length to separation of the lateral jet after which the fluid gets entrained by the ceiling air jet. Consequently, the lower the momentum of the lateral air jets is, the sooner it separates. In the following this effect is named as jet-jet interaction.

4.1.2. Cooling case

Under cooling conditions the influence of the thermal convection on the forced convection can be investigated. For a direct comparison to Fig. 4 (isothermal case) the average velocity field obtained under cooling conditions for configuration A 50/50 is presented in Fig. 6.

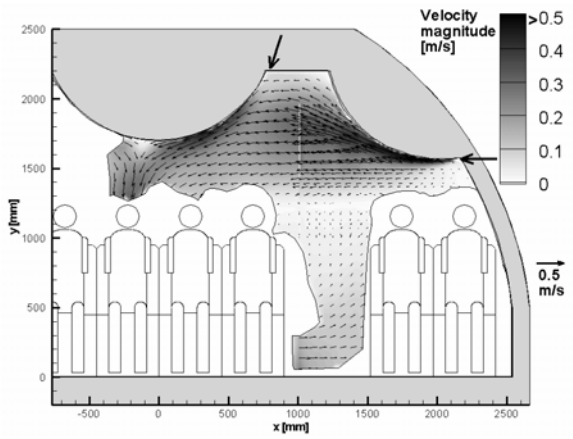

FIG 6. Mean velocity distribution of the air flow in the aircraft passenger cabin mock-up for configuration A 50/50 studied with large-scale 2C-2D PIV under cooling conditions.

It can be observed that compared to the isothermal case the laterally injected air jet separates earlier and spreads out in a wider region. Additionally to the jet-jet interaction the interaction of the buoyant flow with the jet leads to an earlier separation in the cooling case. Decreasing the volume flow rate of the lateral air jet again supports separation due to the lower momentum of the jet.

The RMS velocity fluctuations shown in Fig. 7 for configuration A 50/50, highlight the instationary behaviour of the separation point/line of the lateral air jet at the overhead bin contour. In this respect a more homogeneous RMS distribution, if compared to the isothermal case, with RMS values of up 0.12 m/s in the spreading area of the jet is found. The instationary behaviour of the separation point/line is a result of the complex counteraction of the lateral air jet and the thermal plumes which originate from the passenger dummies and the lateral light band models. Increasing the flow rate of the lateral air stabilizes the lateral jet, since the influence of the thermal plumes decreases.

The maximum velocity magnitude in the air jet area is smaller for the isothermal cases than for the cooling case for the lower lateral flow rates (A 50/50 and A 67/33) and larger for the higher flow rate (A 33/67). There are two explanations for this observation. Firstly, the lateral air jet is accelerated by rising thermal plumes forming a mixed convection roll and secondly, the velocity of the rising jet is reduced due to negative buoyancy forces. Both effects are counteracting but the latter is more effective on higher lateral air flow rates since the temperature difference to the surrounding fluid i.e. the negative buoyancy forces are reduced more slowly.

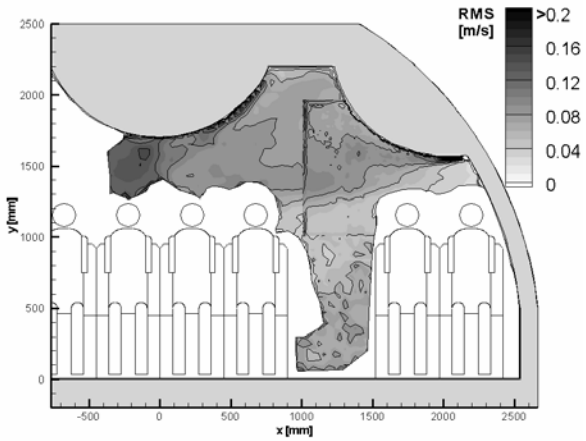

FIG 7. RMS velocity fluctuations of the air flow in the aircraft passenger cabin mock-up for configuration A 50/50 studied with large-scale 2C-2D PIV under cooling conditions.

For configuration A 50/50 the contours of the temperature field together with superimposed velocity vectors are shown in Fig. 8. The pathways of the jets in the cabin mock-up are obvious visible due to the lower temperature, i.e. temperature difference.

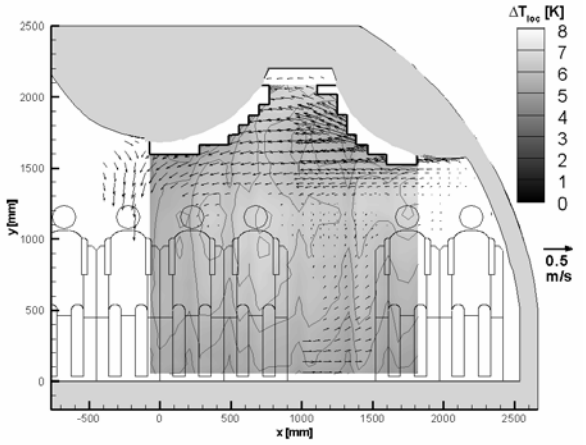

FIG 8. Contours of the averaged temperature field and superimposed velocity vectorss for configuration A 50/50 under cooling conditions.

The parameter study reveals that the temperature in the upper cabin area decreases if the flow rate of the lateral air jet is increased. This is concluded from the temperature profiles at x = 1120 mm in Fig. 9. That the temperature increase from 5.5 K to 7.1 K for the lower lateral air flow rates is due the fact that less heat is removed by the lateral air jet in the upper region. Surprisingly the temperature values in the vicinity of the passenger increase only by 0.5 K when changing to configuration A 67/33 whereas the lateral air flow rate is the lowest, see Fig. 9

Furthermore the temperature values in the cabin centre (x = 0 mm) decrease for increasing flow rates of the ceiling air inlet, as presented in Fig. 10. With higher ceiling air inlet flow rates more cold air has to travel a shorter way and hence has less time for mixing with the warmer surrounding fluid. The result is up to 0.5 K lower

temperatures values in the area above the passengers seated in the cabin centre.

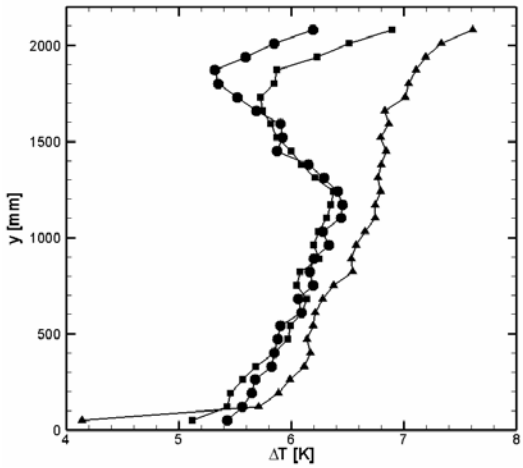

FIG 9. Temperature profiles at x = 1120 mm for configuration A. Triangles: A 67/33, Squares: A 50/50, Circles: A 33/67

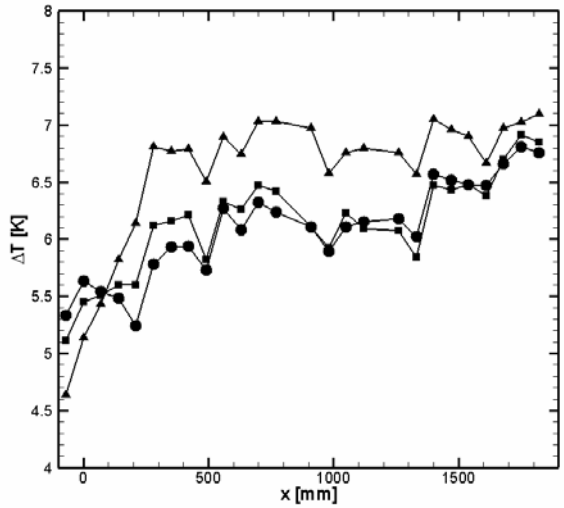

FIG 10. Temperature profiles at y = 1380 mm for configuration A. Triangles: A 67/33, Squares: A 50/50, Circles: A 33/67

4.2. Results for Configuration B

4.2.1. Isothermal case

For configuration B only the ceiling air inlets were operated. To provide an overview of flow field first the averaged velocity magnitude field for the isothermal case and configuration B 67/33 is presented in Fig. 11. Additionally, in Fig. 12 the corresponding RMS velocity fluctuations are shown.

The supplied air jets attach to the overhead bin due to the Coanda effect. In the middle of the cabin the visible air jet at the central overhead bin meets its counterpart from the left cabin side forming a stagnation point. Both jets separate at the contour, merge and descend to the cabin floor, where a second stagnation point develops. There the jets are split in two parts and approach the air outlets. The jet at the outer overhead bin behaves differently. After following the contour the air jet separates and is descends to the floor due to the above explained jet-jet interaction.

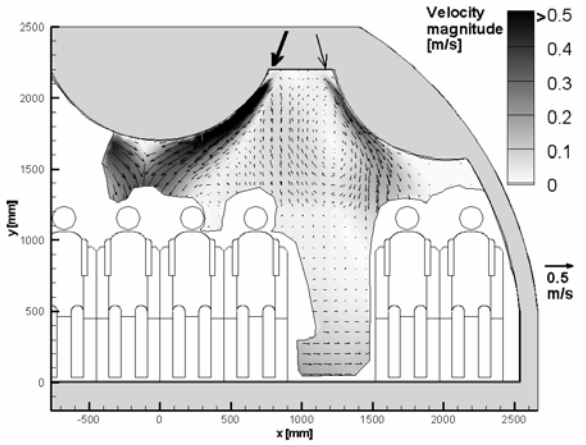

FIG 11. Mean velocity distribution of the air flow in the aircraft passenger cabin mock-up for configuration B 67/33 studied with large-scale 2C-2D PIV under isothermal conditions

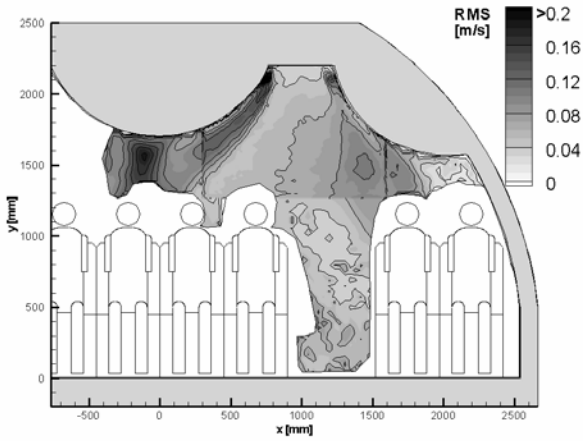

FIG 12. RMS velocity fluctuations of the air flow in the aircraft passenger cabin mock-up for configuration B 67/33 studied with large-scale 2C-2D PIV under isothermal conditions

The RMS values obtained for this configuration (Fig. 12) reflects that the two air jets coming from the inner ceiling air inlets are highly instationary above the passenger heads. This was also observed for configuration A for which high RMS values (up to 0.18 m/s) were found close to the stagnation point.

Separation of the air flow at the contour takes place sooner for lower outer air jet flow rates due to the decrease of jet momentum. Furthermore it was found that the central ceiling air jet does not separate prematurely for lower air flow rates. But, at very low air flow rates of the inner air jet (configuration B 33/67) the flow field seems to become three-dimensional since in the two dimensional cross section shown in Fig. 13 continuity is not fulfilled anymore.

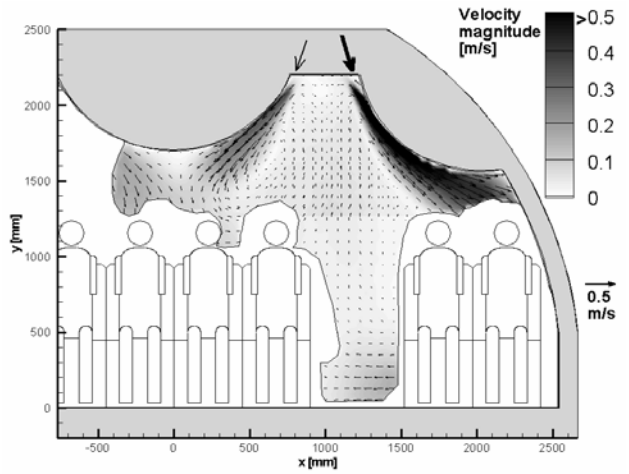

FIG 13. Mean velocity distribution of the air flow in the aircraft passenger cabin mock-up for configuration B 33/67 studied with large-scale 2C-2D PIV under isothermal conditions

4.2.2. Cooling case

Under cooling conditions the flow field is noticeably affected by thermal convection. In Fig. 14 the averaged velocity magnitude field obtained under cooling conditions for configuration B 67/33 is shown. The corresponding distribution of RMS velocity fluctuations are presented in Fig. 15.

The air jet being supplied at the central overhead bin qualitatively behaves just as in the isothermal case. Though, the velocity magnitude of the air jet increases, as shown in Fig. 14. The reason is negative buoyancy forces which accelerate the air jet. Compared to the isothermal flow case in Fig. 11 the air jet at the contour of the outer overhead bin separates earlier under cooling conditions. Besides, the air jet seems to spread out in two directions. The large RMS values (up to 0.2 m/s in Fig. 15) reveal that the separation point/line moves along the contour. Again (see configuration A) an instability originating from counteracting effects like the rising of thermal plumes, negative buoyancy forces acting on the outer air jet and the jet-jet interaction induces the movement of the separation point/line along the contour.

In contrast to the test case B 33/67 (the lowest investigated flow rate of central ceiling air jet), for configuration B 67/33 the jet separates directly after entering the cabin and is entrained by the outer air jet. Although the volume flow rate is enlarged due to entrainment of the other jet the velocity magnitude is lower than in the isothermal case. This is just the opposite behaviour as for configuration B 67/33 for which the velocity magnitude was increased due to the negative buoyancy forces acting on the jet. Here the influence of the thermal plumes is larger than the increase of negative buoyancy forces due to additionally generated thermal plumes by the lateral light band models.

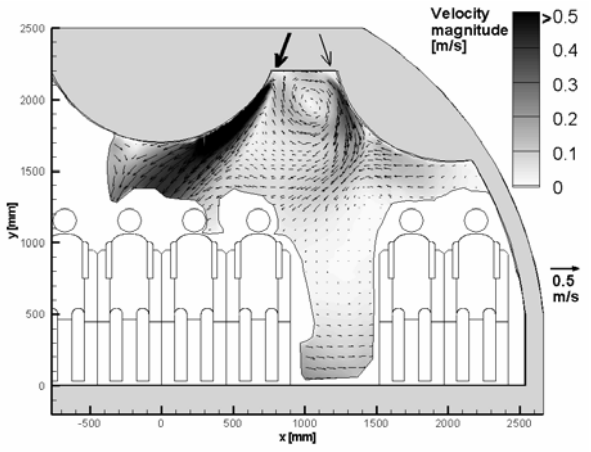

FIG 14. Mean velocity distribution of the air flow in the aircraft passenger cabin mock-up for configuration B 67/33 studied with large-scale 2C-2D PIV under cooling conditions

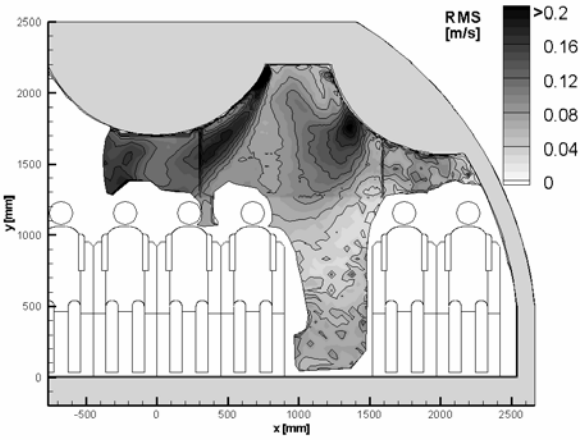

FIG 15. RMS velocity fluctuations of the air flow in the aircraft passenger cabin mock-up for configuration B 67/33 studied with large-scale 2C-2D PIV under cooling conditions

The measured temperature field for configuration B 67/33 is depicted in Fig. 16. Temperature values as low as 4.5 K below the mean cabin temperature are observed in the pathway of the central ceiling air jet. Above the heads of the passenger dummies in one half of the cabin a warmer region of up to 6.8 K above mean develops due to the low heat exchange in this area.

The comparison of parameter variation in Fig. 17 reveals that regions not crossed by the air jets exhibit temperature distribution varying only up to 0.2 K.. Only in the outer cabin area the temperature is increased slightly due the heat input of the lateral light band model at low flow rates from the outer air inlet.

Furthermore the change of the ventilation conditions, i.e. lower flow rates at the central air inlet and the higher flow rates at the outer air inlets, provoke that the air in the area of the passengers is up to 0.6 K colder as presented in Fig. 18.

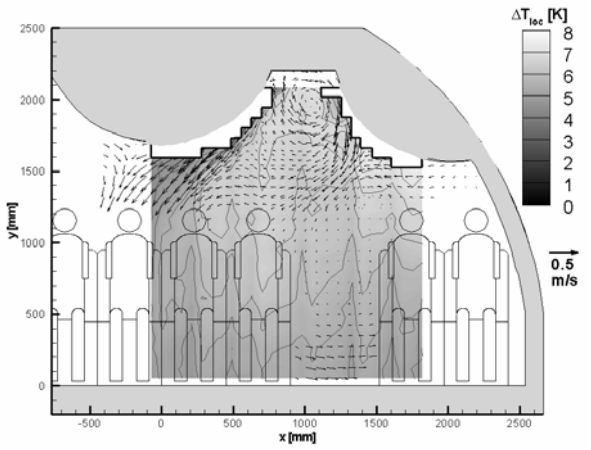

FIG 16. Contours of the averaged temperature field and superimposed velocity vectors for configuration A 50/50 under cooling conditions

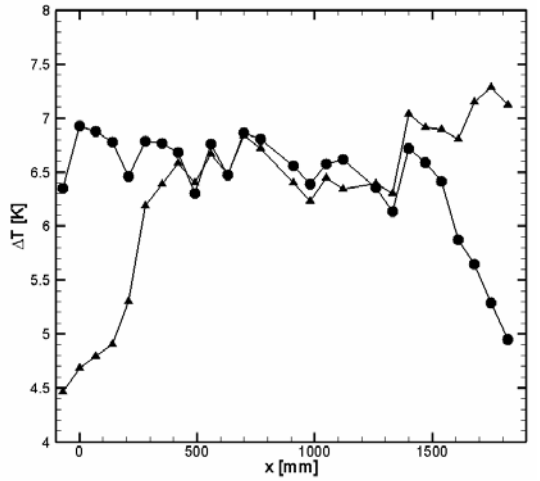

FIG 17. Temperature profile at y = 1380 mm for configuration B. Triangles: B 67/33, Squares: B 50/50, Circles: B 33/67

PIV of the flow for configuration B 50/50 under cooling conditions were performed twice with a recording frequency of 2.5 Hz over 64 s in order study effects associated with the temperature drift during one measurement. The temperature difference ΔT between the averaged cabin temperature and the temperature of the supplied air was approximately 6.15 K. The averaged velocity magnitude field of the first measurement and the corresponding RMS values are shown in Fig. 19 and Fig. 20, respectively.

Both visible air jets are attached at the respective overhead bin and follow the contour until they separate. The RMS values (Fig. 20) reveal that the separation points/lines of both jets are moving along the overhead bin contours generating the wide air jets which descend to the cabin floor.

The averaged velocity field obtained in the second measurement conducted two minutes later than the first is presented in Fig. 21 and RMS values in Fig. 22.

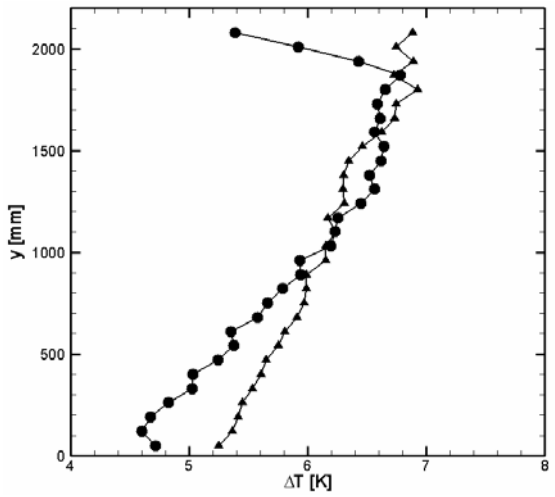

FIG 18. Temperature profile at x = 1120 mm for Configuration B. Triangles: B 67/33, Squares: B 50/50, Circles: B 33/67

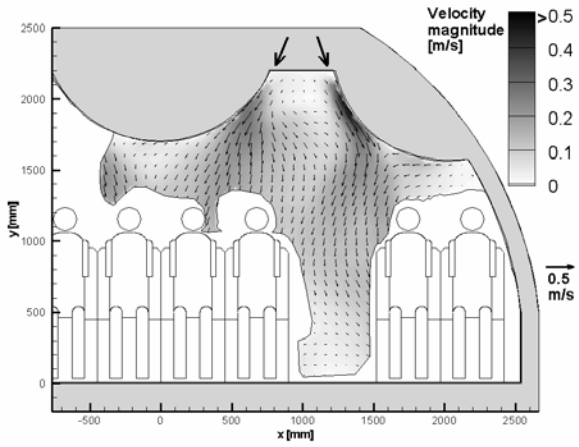

FIG 19. Mean velocity distribution of the air flow in the aircraft passenger cabin mock-up for configuration B 50/50 under cooling conditions first PIV series

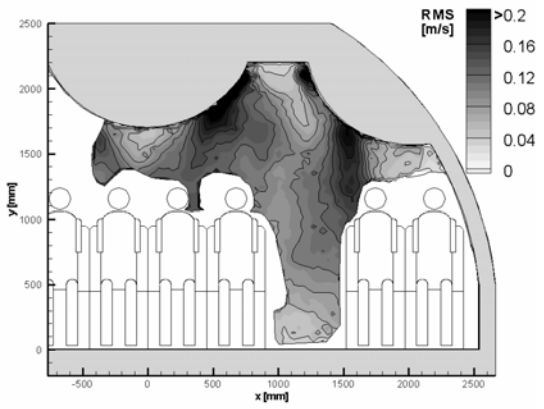

FIG 20. RMS velocity fluctuations of the air flow in the aircraft passenger cabin mock-up for configuration B 50/50 under cooling conditions first PIV series

Obviously, the flow field differs from the one of the first measurement shown in Fig. 19. The air jet at the central overhead bin separates much earlier and is directly entrained by the outer air jet. The remaining jet follows the

outer contour until it also separates. The maximum RMS values of up to 0.09 m/s in the path of the jets reveal that the separation point/line of the central overhead bin air jet does not move along the contour as it was observed in the first measurement.

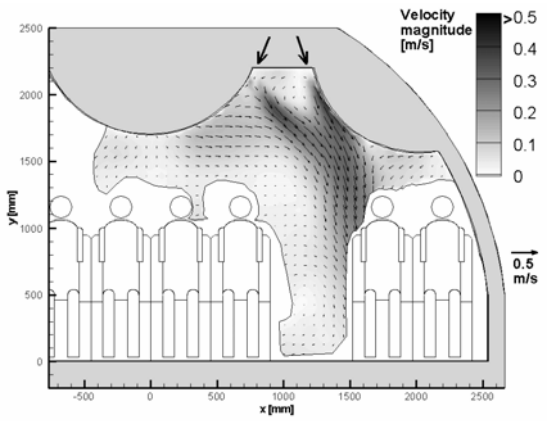

FIG 21. Mean velocity distribution of the air flow in the aircraft passenger cabin mock-up for configuration B 50/50 under cooling conditions second PIV series

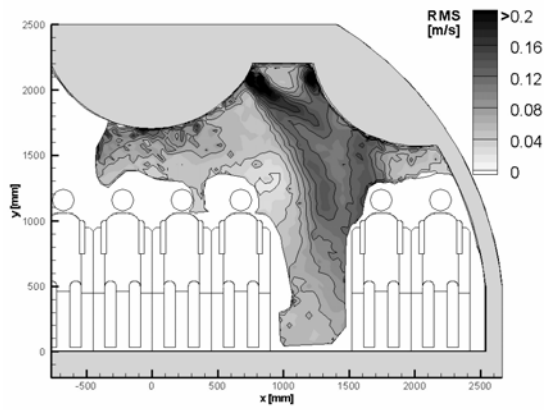

FIG 22. RMS velocity fluctuations of the air flow in the aircraft passenger cabin mock-up for configuration B 50/50 under cooling conditions second PIV series

In order to analyse if the flow topology between the two measurements was changing due to flow instability we additionally measured the temperature distribution in a horizontal line at y = 1520 mm over a time period of more than nine hours. As mentioned above the mean temperature within the mock-up reaches only a quasi-stationary state meaning that the temperature distribution in the horizontal line could be measured as function of the temperature difference ΔT. In Fig. 23 the time variation of the temperature difference ΔT during a measurement period is shown.

The temperature contour plot obtained in the long time measurement is shown in Fig. 24. During the first period of the measurement (t < 2500 s) the temperature distribution is more or less reflected by a horizontal line. With increasing temperature difference ΔT the spreading areas of the jets remain colder (t > 2500 s). Shortly before 18000 s when the temperature difference ΔT = 6.8 K the temperature vales between 100 mm < x < 550 mm increases from an averaged temperature of 25.3°C by approximately 1.7 K. Additionally the spreading area of the outer air jet nearly doubles. At this time the topology of the flow field changes.

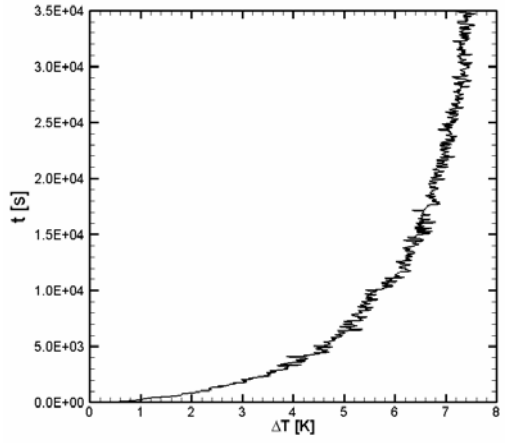

FIG 23. Development of the temperature difference of the supplied air ΔT with respect to the average cabin temperature.

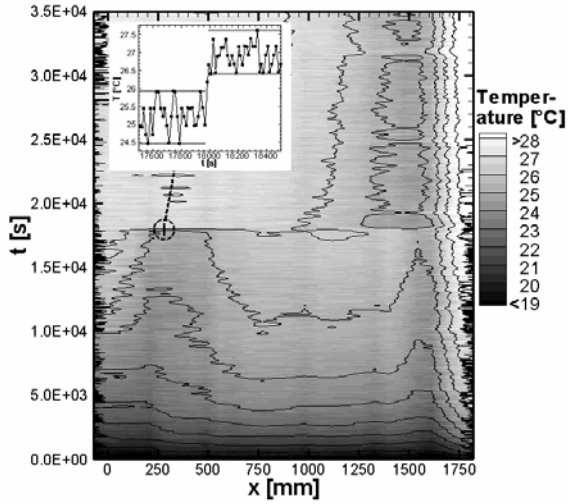

FIG 24. Temperature distribution on a horizontal line at y = 1520 mm and in the inset the temperature signal at x = 280 mm for ±500 s

In the inset of Fig. 24 the temperature signal of the sensor at x = 280 mm is depicted for a time interval of ± 500 s in which air circulation changes. It is further observed that the corresponding change in the temperature field takes place in a short time period of less than one minute. The fact that the temperature difference ΔT increases only by 0.03 K (inset of Fig. 24) indicates a change of the large scale flow due to a flow instability. The instability is a result of the complex interaction of the descending air jets, the rising thermal plumes influenced by negative buoyancy forces and the jet-jet interaction. Furthermore, it must be noticed that the temperature difference ΔT is 0.6 K higher in the long time temperature measurement than in the PIV measurements due to two reasons. Firstly, the flow configuration in the cabin mock-up was changed several times a day and secondly, the experimentalists entered the cabin mock-up before the measurements, e.g. for checking the soap bubble nozzles. This was not the case in the long time temperature measurements.

The lesson learned of the above measurement is that one should avoid disturbing the flow field if it might be unstable. Small disturbance like walking passengers in the aisle can cause a global change of the field resulting probably in decreasing the thermal comfort of passengers.

5. CONCLUSIONS

Mixed convection has been investigated in a passenger aircraft cabin mock-up by means of PIV and temperature measurements. Two different air inlet configurations were considered in an extensive parameter study. For both configurations the air inlet flow rates were varied at a constant flow exchange rate.

It was demonstrated that several physical fluid effects have a large impact on the flow field in an aircraft cabin. To summaries, these effects are the jet-jet interaction, negative buoyancy forces and rising thermal plumes that influence the pathway of the supplied air jets. Premature separation from the overhead bin contours is caused by these effects especially at lower flow rates of the air jet. It is shown that the impact of these effects differ strongly depending on the ventilation configuration and settings. From the discussion of the parameter study it could be concluded that understanding these effects is crucial for the design of air conditioning systems of a passenger aircraft and their components if the thermal comfort of passengers is to be guaranteed.

Furthermore it was found that under certain conditions flow instabilities can induce a global change of the large scale air circulation. When operating aircrafts such settings should be avoided to guarantee the thermal comfort throughout the whole flight.

REFERENCES

[1] J. Bosbach, M. Kühn, C. Wagner (2007). Large scale PIV…. Experiments in Fluids …in preparation
[2] J. Bosbach, J. Penneçot, C. Wagner, M. Raffel, T. Lerche and S. Repp (2006). Experimental and numerical simulation of turbulent ventilation in aircraft cabin. Energy. 31:694-705.References.
[3] D. Müller, B. Müller and U. Renz (2001). Three-dimensional particle streak tracking (PST) velocimetry measurements of heat exchanger inlet flow. Experiments in Fluids. 30:645-656.
[4] M. Raffel, C. Willert and J. Kompenhans (1997). Particle Image Velocimetry - A practical Guide. Berlin: Springer-Verlag.
[5] R.H.G. Müller, T. Scherer, T. Rötger, O. Schaumann, M. Markwart (1997). Large body aircraft cabin a/c flow measurement by helium bubble tracking. Journal of Flow Visualization & Image Processing. 4:295-306.
[6] Y. Zhang, Y. Sun, A. Wang, J.L. Topmiller and J.S. Benett (2005). Experimental characterization of airflows in aircraft cabins, Part II: Results and research recommendation. ASHRAE Transactions. 111:53-59.
[7] Y. Sun, Y. Zhang, A. Wang, J.L. Topmiller and J.S. Bennet (2005). Experimental characterization of airflows in aircraft cabins, Part I: Experimental System and measurement procedure. ASHRAE Transactions. 111:45-52.
[8] R.H.G. Müller, , H. Flögel, T. Scherer, O. Schaumann and U. Buchholz (2000). Investigation of large scale low speed air condition flow using PIV. Proceedings of 9th International Symposium on Flow Visualization, Edinburgh, August 22-25.
[9] H. Mo, M.H. Hosni and B.W. Jones (2003). Application of particle image velocimetry for measurement of the airflow characteristics in an aircraft cabin. ASHRAE Transactions. 109:101-110.
[10] C.-H. Lin, T.T. Wu, R.H. Horstman, P.A. Lebbin, M.H. Hosni, B.W. Jones and B.T. Beck (2006). Comparison of large eddy simulation predictions with particle image velocimetry data for airflow in a generic cabin model. HVAC&R Research. 12(3c):935-951.
[11] C.-H. Lin, R.H. Horstman, M.F. Ahlers, L.M. Sedgwick, K.H. Dunn, J.L. Topmiller, J.S. Bennett and S. Wirogo (2005a). Numerical simulation of airflow and airborn pathogen transport in aircraft cabins – Part I: Numerical simulation of the flow field. ASHRAE Transactions. 111:755-763.
[12] C.-H. Lin, R.H. Horstman, M.F. Ahlers, L.M. Sedgwick, K.H. Dunn, J.L. Topmiller, J.S. Bennett and S. Wirogo (2005b). Numerical simulation of airflow and airborn pathogen transport in aircraft cabins – Part II: Numerical simulation of airborne pathogen transport. ASHRAE Transactions. 111:764-768.
[13] G. Günther, J. Bosbach, J. Penneçot, C. Wagner, T. Lerche and I. Gores (2006). Experimental and numerical simulations of idealized aircraft cabin flows. Aerospace Science and Technology. 10:563-573.
[14] T. Mizumo and M.J. Warfield (1992). Development of three-dimensional thermal airflow analysis computer program and verification test. ASHRAE Transactions. 98:329-338.
[15] A. Singh, M.H. Hosni and R.H. Horstman (2002). Numerical simulation of airflow in an aircraft cabin section. ASHRAE Transactions. 108:1005-1013.
[16] A.W. DeJager and D.B. Lytle (1992). Commercial airplane air distribution system development through the use of computational fluid dynamics. Proceedings of 1992 Aerospace Design Conference, Irvin, February 3-6.